HHS Public Access

Author manuscript

Acad Radiol. Author manuscript; available in PMC 2017 December 01.

Published in final edited form as:

Acad Radiol. 2016 December ; 23(12): 1521–1531. doi:10.1016/j.acra.2016.07.014.

Using Hyperpolarized ^{129}Xe MRI to Quantify the Pulmonary Ventilation Distribution

Mu He, MS[1,2], **Bastiaan Driehuys, PhD**[1,2,3,4], **Loretta G. Que, MD**[5], and **Yuh-Chin T. Huang, MD, MHS**[5]

[1]Center for In Vivo Microscopy, Duke University Medical Center, Durham, NC, USA

[2]Department of Electrical and Computer Engineering, Duke University, Durham, NC, USA

[3]Department of Biomedical Engineering, Duke University, Durham, NC, USA

[4]Department of Radiology, Duke University Medical Center, Durham, NC, USA

[5]Department of Medicine, Duke University Medical Center, Durham, NC, USA

Abstract

Background—Ventilation heterogeneity is impossible to detect with spirometry. Alternatively, pulmonary ventilation can be imaged 3-dimensionally using inhaled ^{129}Xe MRI. To date such images have been quantified primarily based on ventilation defects. Here, we introduce a robust means to transform ^{129}Xe MRI scans such that the underlying ventilation distribution and its heterogeneity can be quantified.

Methods—Quantitative ^{129}Xe ventilation MRI was conducted in 12 younger (24.7±5.2 yrs), and 10 older (62.2±7.2 yrs) healthy individuals, as well as 9 younger (25.9±6.4 yrs) and 10 older (63.2±6.1 yrs) asthmatics. The younger healthy population was used to establish a reference ventilation distribution and thresholds for 6 intensity bins. These were used to display and quantify regions of ventilation defect (VDR), low ventilation (LVR) and high ventilation (HVR).

Results—The ventilation distribution in young subjects was roughly Gaussian with a mean and SD of 0.52±0.18, resulting in VDR=2.1±1.3%, LVR=15.6±5.4% and HVR=17.4±3.1%. Older healthy volunteers exhibited a significantly right-skewed distribution (0.46±0.20, p=0.034), resulting in significantly increased VDR (7.0±4.8%, p=0.008) and LVR (24.5±11.5%, p=0.025). In the asthmatics, VDR and LVR increased in the older population, and HVR was significantly reduced (13.5±4.6% vs 18.9±4.5%, p=0.009). Quantitative ^{129}Xe MRI also revealed different ventilation distribution patterns in response to albuterol in two asthmatics with normal FEV1.

Corresponding Author: Yuh-Chin T. Huang, MD, MHS., 1821 Hillandale Road, Suite 25A, Duke University Medical Center, Durham, NC 27710, Phone: 919-684-3069, FAX: 919-684-3199, huang002@mc.duke.edu.

Authors' contributions: All authors designed the method in this study. MH, and YTH performed the statistical analysis. All authors interpreted the data, prepared the manuscript, and drafted the article. All authors approved this manuscript in its final form.

Conflict of Interest: MH, LGQ, YTH have no conflict of interest relevant to the study. BD is founder of Polarean, which is involved in the commercialization of hyperpolarized ^{129}Xe MRI technology.

Conclusions—Quantitative ^{129}Xe MRI provides a robust and objective means to display and quantify the pulmonary ventilation distribution, even in subjects who have airway function impairment not appreciated by spirometry.

Keywords

Asthma; aging; albuterol

INTRODUCTION

The distribution of ventilation is known to be non-uniform in healthy lungs (1–6), and this heterogeneity increases with age and disease. Ventilation heterogeneity is impossible to quantify using spirometry because it measures the lung as a single unit and is insensitive to pathology in the small airways — the so-called "silent zone". Alternative approaches include using the multiple-breath-nitrogen washout (MBNW) test to determine the distribution of specific ventilation (2, 7), the lung clearance index (LCI) (8–11), or the multiple inert gas elimination technique (MIGET) to quantify the ventilation-perfusion relationship (6); however, none of these tests provides spatial information. Alternatively, imaging methods such as computed tomography (CT) delineate spatial changes in lung structures that may allow ventilation abnormalities to be inferred. However, CT does not directly measure ventilation and its radiation dose limits some longitudinal studies.

Recently, MR imaging techniques have emerged that enable direct detection of inhaled gases, such as oxygen (12–14), perfluorinated gases (15, 16), and hyperpolarized (HP) ^{3}He (4, 17, 18). They enable visualization of ventilation defects that have been shown to correlate with airway tone (4, 19–21) and airways abnormalities (22). HP ^{3}He MRI readily depicts regional ventilation heterogeneity in patients with pulmonary obstructive diseases (23). More recently, ^{129}Xe gas has emerged as the most promising alternative to address dwindling supplies of ^{3}He (24–26). ^{129}Xe MRI appears to more readily detect ventilation defects than ^{3}He MRI (21, 27) and has been used to visualize elimination of ventilation defects after bronchodilator administration (28).

However, the analysis of ^{129}Xe magnetic resonance imaging (MRI) scans has yet to fully capture the entire pulmonary ventilation distribution. Most methods have focused on quantifying the ventilation defect percentage (VDP), the fraction of the lung with ventilation below an arbitrary threshold (29–31). While VDP quantifies the most severely affected lung units, its definition is not robust. Moreover, VDP does not report on lung units with mild to moderate impairment, or increased ventilation. This has led to efforts to extend beyond the VDP, including heterogeneity (4, 25, 28). Recently, more sophisticated methods such as the hierarchical k-means clustering algorithm have been introduced (30) to derive 5 different ventilation levels from ^{3}He MRI and these were quantified in asthmatics (32). For ^{129}Xe MRI, our own group recently introduced a method to rescale image intensity into 4 bins (31) and have shown VDP derived from such maps to be reproducible to ±1.52% (33). However, it has not yet been determined how these maps could be used to recover the pulmonary ventilation distribution.

Here, we present a novel approach to analyzing ^{129}Xe MRI scans that combines image histogram characterization and linear binning maps to more comprehensively map and quantify the underlying distribution of pulmonary ventilation. We illustrate its utility by detecting abnormalities in the scans from older normal subjects with normal spirometry. We subsequently characterize differences in ventilation distribution in older and younger asthmatics and illustrate the way in which it is altered by bronchodilator therapy.

METHODS

Subjects

We recruited 12 healthy young (18–30 years old) and 10 healthy older (50–70 years old) individuals who were nonsmokers, with FEV1>85% according to ethnically appropriate reference tables and FEV1/FVC>0.7. We also recruited 9 younger (18–30 years old) and 10 older (50–70 years old) patients with mild intermittent asthma. Each subject provided informed consent to participate in the study protocol.

Image Acquisition

All MR scans were performed on a 1.5 T GE Healthcare EXCITE 15M4 MR system, using protocols described previously (31). Briefly, subjects were fitted in the supine position with a flexible chest coil (Clinical MR Solutions, Brookfield, WI) that was tuned to the 17.66 MHz ^{129}Xe frequency and proton-blocked to permit acquiring anatomical scans using the ^{1}H body coil. After the initial localizer and thoracic cavity scans (described below), all subjects underwent ^{129}Xe ventilation MRI after inhaling a dose equivalent of DE=71 ml HP ^{129}Xe filled to 1 liter total volume with helium buffer gas (34). Some asthmatics underwent an additional ^{129}Xe ventilation MRI scans after 4 puffs of albuterol with lower DE = 24 ml, ten minutes after the first ^{129}Xe MRI scan. Scan parameters (71 ml/24 ml DE) were: fast spoiled gradient echo, field of view (FOV)=40/48 cm, matrix=128×(90–128)/64×64, slice thickness=12.5 mm, bandwidth (BW)=8.3 kHz, flip angle=7–10°, repetition time (TR)/echo time (TE)=8.1/1.9 ms, and slices were acquired in anterior to posterior order (34). The ^{129}Xe GRE ventilation images were analyzed in the context of a thoracic cavity image acquired of the same slices using a breath-hold ^{1}H steady state free precession (SSFP) imaging sequence using the scanner's body coil. For this anatomical reference scan, subjects were in the same position as for ^{129}Xe MRI and inhaled a 1-liter bag of room air. The ^{1}H images were then acquired with FOV=40 cm, matrix=192×192, slice thickness=12.5 mm, flip angle=45°, TR/TE=2.8/1.2 ms, and BW=125 kHz. All ^{1}H and ^{129}Xe MR images were reconstructed directly from the scanner and exported as 256×256×14 DICOM slices for analysis.

Image Analysis

Image analysis employed an extension of the method (31) we previously introduced in order to transform grey-scale ^{129}Xe MR images into maps that depict various levels of signal intensity. As illustrated in Figure 1, this method overcomes the lack of absolute MR signal scale (unlike Hounsfield units in CT) by analyzing the ^{129}Xe image in the context of a thoracic cavity mask and using the top percentile of intensities to rescale the image histogram to range from 0–1. In addition to correcting for the effects of vasculature and ^{129}Xe coil bias field, we applied two additional technical extensions. We now retain

signal from the major airways prior to histogram rescaling, but remove them prior to quantitative reporting; these airways replenish fully with each breath and contribute the top percentile of intensities. Furthermore, we erode the thoracic cavity mask by 1 pixel to minimize false defects near the lung borders.

To establish an unbiased reference distribution we first characterized the averaged rescaled ^{129}Xe intensity histograms from healthy young volunteers. Of these 12 younger volunteers scanned, images from 10 were deemed to exhibit no ventilation defects by visual inspection. From these subjects, an averaged rescaled intensity histogram was generated, and its mean and standard deviation (SD) were used to define the threshold intensities for the ensuing 6-bin maps. The mean of this distribution defined the boundary between bins 3 and 4, which were classified as the normally ventilated regions. Each bin was assigned a width of 1 SD. The lowest intensity bin was identified as the ventilation defect region (VDR), followed by the low ventilation region (LVR), while the highest two bins were combined to form the high ventilation region (HVR). These same definitions were then used to analyze all subsequent images by classifying each pixel into one of the 6 bins. In addition, the coefficient of variation (CV) of each rescaled distribution was calculated by taking the ratio of its SD to its mean. Each image was then displayed in its original grey-scale, as a 6-bin color map, and with its associated histogram depicting the rescaled intensity distribution relative to that of the young healthy reference population.

Statistical Methods

Pulmonary function tests and binning map quantification were tested for significant differences between age and asthmatic groups using a one-tailed student's t-test. This approach was justified given that previous ^{3}He literature had shown that ventilation defects increase and lung function declines as age increases (21). Skewness of the distribution was assessed by Pearson's moment coefficient of skewness. Differences were considered significant when the probability of a type 1 error was 0.05 or less. All statistical analyses were performed using JMP 11 (SAS Institute Inc., Cary, NC).

RESULTS

Study population

After excluding 2 healthy subjects with ventilation defects, the study included 10 younger healthy subjects (age: 24.7±5.2 years, FEV1: 103.9±13.3% predicted), 10 older healthy subjects (age: 62.2±7.2 years, FEV1: 97.7±13.9% predicted), 9 younger asthmatics (age: 25.9±6.4 years, FEV1: 84.3±16.3 predicted), and 10 older asthmatics (age: 63.2±6.1 years, FEV1: 79.5±22.4 predicted).

Distribution of ventilation in young healthy subjects

The rescaled ^{129}Xe ventilation distributions for each of the healthy young individuals are shown in Figure 2; each exhibited a nearly Gaussian shape and when all 10 were combined, the distribution had a mean of 0.52 and SD of 0.18. These parameters generated thresholds for the binning maps of 0.16, 0.34, 0.52, 0.70 and 0.88. When these thresholds were applied to the healthy younger subject population, they exhibited volume fractions of

VDR=2.1±1.3%, LVR=15.6±5.4% and HVR=17.4±3.1%. For these young healthy volunteers, the average skewness of the ventilation distribution was 0.0±0.1 and its CV was 0.37±0.04.

Effects of Age

Figure 3A compares the images, binning maps and distribution histograms of a 27-year-old healthy subject with FEV1=86% (Using south Asian reference table (35)) to those of a 58-year-old healthy subject with FEV1=102%. The healthy younger subject exhibits a relatively homogenous ventilation distribution with the bulk of the voxels falling within the central green bins and some intensity in the HDR region. VDR and LVR (red and orange bins) were similar to reference, and CV was 0.31. By contrast, the older subject, despite having normal FEV1, exhibits elevated VDR (9.4%) and LVR (32.2%) visually, as well as increased CV of 0.50. As shown in Figure 3B, this older control exhibited a right-skewed distribution (skewness=0.47) histogram relative to the reference population.

As seen in Figure 4, the aggregate ventilation distribution in the older healthy subjects was right-skewed (skewness=0.36) compared to the younger group, resulting in a significantly lower mean value (0.46±0.08, p=0.034), and a significantly increased SD (0.20±0.01, p=0.017). As a result, this group exhibited a significantly increased VDR (7.0±4.8%, p=0.0076) and LVR (24.5±11.5%, p=0.025) compared to the younger normal reference group. The increased fractions of VDR and LVR appear to have depleted the populations of the two middle bins, while HVR remained close to reference (14.7±7.5%, p=0.20). In this older population, the higher SD, and lower mean of the ventilation distribution also caused heterogeneity to increase, as reflected by a significantly higher CV (0.45±0.09, p=0.014).

Ventilation distribution in older and younger asthmatics

Figure 5 shows representative grey-scale images, 6-bin maps and ventilation distribution histograms for a 36-year-old asthmatic with FEV1=76% and a 68-year-old asthmatic with FEV1=53%. For this example, the younger subject exhibits no significant ventilation defects (VDR=2.1%), and a relatively high fraction of HVR (24.1%). By contrast, the older asthmatic subject exhibits more ventilation defects (VDR=14.0%), and a significantly diminished HVR (9.3%). As shown in Figure 5A, this young asthmatic had a distribution histogram that was similar, and even slightly left-skewed (skewness=−0.1) relative to the reference population. By contrast, in the older asthmatic the histogram was right-skewed (skewness=0.56), with substantial depletion of the higher intensity bins (Figure 5B).

Comparing the younger and older asthmatic groups (Figure 6) reveals not only that, in the older asthmatics VDR (11.4±9.4%, p=0.02) and LVR (20.2±6.7%, p=0.016) are increased, but also that HVR is significantly diminished (13.5±4.6%, p=0.009). As was the case for older healthy subjects, aging in asthma caused heterogeneity to increase (Skewness=0.06 for younger asthmatics and 0.32 for older asthmatics), resulting in an elevated SD (0.21±0.02, p=0.049), CV (0.48±0.12, p=0.017) and a decreased mean (0.45±0.07, p=0.008) relative to younger asthmatics.

Differences between FEV1 and ^{129}Xe MRI Ventilation Distribution

We subsequently used these methods of characterizing the ^{129}Xe ventilation distribution to illustrate several individual cases in which ^{129}Xe MRI and spirometry convey contrasting pictures of lung function. Shown in Figure 7 are cases of 4 asthmatics - one with normal FEV1, but abnormal ^{129}Xe MRI (Figure 7A), one with abnormal FEV1, but normal ^{129}Xe MRI (Figure 7B), and two with moderate asthma (Figure 7C–D), who have similarly low FEV1, but radically different ventilation patterns. The 69-year-old asthmatic in Figure 7A, had FEV1=90%, but a ventilation distribution that was right-skewed from the reference distribution. This resulted in visible defects and increased VDR (10.4%). By contrast, the 19-year-old asthmatic in (Figure 7B) had FEV1=77%, but a ventilation distribution nearly identical to the reference curve. The subjects in Figures 7C and D had similar FEV1s of 59% and 53%; however, their ventilation distributions bear little resemblance to one another. The subject in 7C exhibits a relatively homogenous ventilation distribution, with the bulk of the voxels falling within the central green bins. This subject exhibits only a slightly elevated VDR (7.9%) while LVR (18.7%) and HVR (15.5%) remained within the normal range. By contrast, the subject in 7D exhibits greatly elevated VDR (35.9%) and LVR (25.8%), while HVR is significantly diminished (5.7%).

Ventilation distribution before and after albuterol treatment

Quantitative ^{129}Xe MRI can also be used to evaluate bronchodilator response in patients with normal FEV1. Figure 8 shows ^{129}Xe MRI and the associated binning analysis in a patient with mild intermittent asthma (FEV1=86%) before and after bronchodilator administration. At baseline, the binning map exhibits high percentages of VDR (13.5%) and LVR (27.8%), especially in the right lower lobe, and somewhat lower than normal HVR of 11.5%. After 4 puffs of albuterol, the patient's FEV1 increased by 15% to 101% predicted (classifying them as a "responder"), and the binning map (Figure 8B) showed a commensurate reduction in both VDR (2.4%) and LVR (15.2%), while HVR increased (17.2%). The associated histogram shifted to higher values and approached the healthy young control distribution. Figure 9 shows a second patient with mild intermittent asthma with FEV1 of 90% predicted before albuterol. For this patient, the binning map at baseline (Figure 9A) exhibited slightly elevated VDR (6.4%), and relatively normal LVR (15.5%) and HVR (18.2%). After albuterol treatment, there was no appreciable change in FEV1 (91% predicted or a "non-responder"). In this patient the ^{129}Xe VDP decreased somewhat (from 6.4% to 3.2%), but LVR actually increased from 15.5% to 23.4% (Figure 9B). This view is more easily grasped by evaluating the patient's ventilation histograms, which paradoxically shifted towards lower values.

DISCUSSION

Clinical application of ^{129}Xe MRI requires accurate quantification and visualization of the ventilation abnormalities. In this study, we report initial results from a novel ^{129}Xe MRI analysis approach that accounts not just for defects, but represents and quantifies the ventilation distribution in its entirety. The essence of the method is to rescale the native ^{129}Xe MR image intensities by their top percentile such that the distribution ranges from 0 to 1. Applying such rescaling to the ^{129}Xe MRI scans from 10 healthy younger

volunteers without visible ventilation defects revealed that their aggregate distribution was nearly Gaussian. From it, a mean and SD could be derived and used to define the thresholds and widths for 6 bins used to generate quantitative color maps. These maps, in turn permit both visualization and quantification of the regions containing absent, low, normal and high ventilation.

This method builds on several previously published HP gas MRI analysis methods. Like those, it readily reports the ventilation defect percentage (VDP) (20, 25, 29, 31, 36), but now replaces subjective thresholds with unbiased ones derived from a well-defined reference population, and reports on the complete ventilation distribution. Moreover, like the hierarchical k-means clustering method, our new approach extends the analysis beyond VDP in order to quantify the remaining aspects of the ventilation distribution (30). However, in our hands, we found the binning approach described here to involve fewer assumptions than k-means, which can be affected by the choice of initial centroids and number of clusters (37). Moreover, the k-means may not perform well in the case of unevenly sized or overlapping clusters (38). The binning approach also connects naturally to physiological principles and may therefore be more intuitive to practicing clinicians.

Using the methods outlined here, we found that young healthy individuals exhibit a narrow ventilation distribution. This agrees qualitatively with ventilation distributions measured by the multiple inert gas elimination technique (1), where the differential blood excretion of soluble inert gases is fit to a 50-compartment model. Our approach can also be loosely related to the imaging-derived calculations of fractional ventilation and specific ventilation. Fractional ventilation measures the turnover of gas on a voxel-by-voxel basis, and typically requires inhalation or exhalation of multiple breaths (39), a series of image registration steps, and numerous corrections to account for polarization losses (40). Such methods were recently used by Horn with ^{3}He MRI to estimate fractional ventilation distributions in 4 healthy subjects and reported r=0.25±0.11 (41). Similarly, Hamedani recently reported r=0.24±0.06 for ^{3}He MRI (42). A closely related measure is specific ventilation (SV), which was measured by Sa, using oxygen-enhanced proton MRI in 8 healthy individuals to have a mean of 0.24–0.42 and an SD of 0.08–0.14 (43). Converting these averages to fractional ventilation using $r=SV/(SV+1)$, yields r~0.25±0.10. Thus, it appears that the ventilation distribution with mean of 0.52±0.18 derived by our relatively simple, but robust rescaling approach, can be loosely related to more rigorous and technically challenging multi-breath measures of fractional ventilation, by a factor of ~0.5.

The 6-bin analysis method proved capable of detecting subtle ventilation changes in older individuals who have normal spirometry. Similar age-related changes have been reported using hyperpolarized ^{3}He MRI by Sheikh, who found ventilation defects in lung periphery in 39 of 52 elderly nonsmokers (44). Such defects can be understood in the context of the aging lung, which undergoes pathological changes, such as degeneration of small airways and loss of tissue support for peripheral airways. These, in turn, lead to increased ventilation heterogeneity and appearance of low VA/Q regions (44–46). In our analysis this is reflected in greater fractions of VDR and LVR that can be appreciated and explained by the right-skewing of the ventilation distribution in older subjects. Such aging-related effects have also been reported by Cardus, who used MIGET to confirm that log SDv increases slightly with

age (46). These age-specific physiological changes will need to be considered when interpreting ventilation distribution results from ^{129}Xe MRI in older individuals.

The ^{129}Xe-derived ventilation distributions in younger and older asthmatics also exhibited significantly different character. While the greater fractions of VDR and LVR seen in older asthmatics is somewhat expected (47), a more striking finding was the significant reduction of HVR in the older vs. younger patients. HVR may correspond to part of the gravity-dependent regions of the lung that naturally receive more ventilation, or may represent regions of the lung that are subserved by collateral airways. Collateral ventilation is an important protective mechanism for minimizing ventilation-perfusion heterogeneity (48, 49). It has been shown using the stop-flow maneuvers by Kaminski, that asthma patients have more narrowing and closure of collateral airways and that closure that was sensitive to challenge with cool-dry air (50). Thus, narrowing of these airways in the older asthmatic patients could explain our observed decrease in HVR. However, the exact pathophysiological determinants relevance of VDR, LVR and HVR require further validation in additional pulmonary phenotypes.

A third example demonstrating sensitivity of ^{129}Xe MRI is given by its ability to detect ventilation abnormalities in mild asthmatics with normal spirometry. Normal PFTs in patients with mild intermittent asthma are not uncommon, indicating that this subgroup has fairly mild and well-controlled airway hyper-reactivity. In our study of 19 asthmatics, 12 were asymptomatic with mild intermittent disease and normal FEV1, and 6 of them exhibited significant ventilation defects. Detecting such defects in asymptomatic individuals has precedent in ^{3}He MRI, where Altes showed peripheral ventilation defects in 7 of 10 asthmatics whose FEV1 ranged from 62% to 126% predicted (23). Building on this, de Lange et al used ^{3}He to study 58 patients with asthma but found no difference in ventilation defect score between patients with mild intermittent asthma and healthy subjects (18). It appears ^{129}Xe may be more sensitive to the entire ventilation distribution than ^{3}He, and analyzing it in its entirety yields insights beyond VDP. Similarly, ^{129}Xe MRI revealed radically different ventilation distributions in patients with similarly low FEV1. This may indicate that the current categories of asthma could benefit from further stratification by ventilation distribution patterns. However, of the 12 mild intermittent asthmatics, 7 of them exhibited a ventilation distribution that was similar to our healthy reference cohort. This similarity and lack of obvious difference in quantitative metrics derived from the histogram, poses difficulties in separating intermittent asthmatics from controls. Further studies will be therefore needed to find signatures that discriminate these subjects, as well as to assess the robustness of this analysis methodology and how well it correlates with other clinical phenotypes (51).

And finally, the sensitivity of ^{129}Xe MRI provides insights into the way ventilation distribution changes in patients with mild intermittent asthma before and after albuterol treatment. In one asthmatic exhibiting a 15% improvement in FEV1 after albuterol, ^{129}Xe MRI showed a ventilation distribution that shifted towards higher values, causing VDR and LVR to decrease while HVR increased. These changes were consistent with bronchodilation at the narrowed (or more diseased) airways and thus move the “choke point” downstream (toward the mouth) (52). Such reversibility of ventilation defects has been previously

visualized by ^{3}He and ^{129}Xe MRI in asthma patients who responded to bronchodilator (28, 53, 54). Unique to our study is illustration of an asthmatic with normal baseline FEV1, and no FEV1 response after bronchodilator use, where ^{129}Xe MRI reveals substantial redistribution of ventilation. In this case, VDR was reduced, but this was accompanied by an increase in LVR, suggesting that bronchodilation may have also occurred in more normal (less affected) and distal airways. The changes, however, were insufficient to shift the choke point downstream (52). Thus, ^{129}Xe MRI ventilation distribution may serve as a more sensitive endpoint for describing albuterol response than spirometry. ^{129}Xe MRI could also be used to investigate the mechanisms for therapeutic response in patients with obstructive airway pathology. Because the technique is inherently non-invasive, it is well suited to repeat application on any desired time scale. Changes in ventilation distribution without changes in spirometry have been demonstrated when ventilation heterogeneity was quantified by more sensitive techniques, such as MBNW (55) and MIGET (53). Moreover, LCI derived from the MBNW test is the earliest measurement for small airway dysfunction in cystic fibrosis (8, 9, 56); Macleod et al (55) reported a significantly elevated LCI suggesting ventilation heterogeneity in asthmatic children compared to age matched healthy children. So far, although LCI was primarily applied to pediatric populations population (10, 55), it could be the most appropriate metric against which to compare ^{129}Xe MRI in future studies.

In summary, the analysis of ^{129}Xe MRI scans by histogram rescaling and objectively generated 6-bin maps represents a novel way to more comprehensively analyze the ventilation distribution and holds significant promise for more sensitively detecting ventilation abnormalities under a variety of baseline conditions and stimuli. This analysis method has the sensitivity to detect regional changes in ventilation, even when spirometry does not. With additional, larger studies, this analysis methodology may prove broadly useful for more sensitive regional assessment of obstructive lung disease and detection of therapeutic efficacy.

Acknowledgments

Funding support: R01HL105643, R01HL126771, P41 EB015897, The Duke Private Diagnostic Clinic ENhanced Academics in a Basic Laboratory Environment (ENABLE) Award.

References

1. Wagner PD, Laravuso RB, Uhl RR, West JB. Continuous distributions of ventilation-perfusion ratios in normal subjects breathing air and 100 per cent O2. J Clin Invest. 1974; 54(1):54–68. [PubMed: 4601004]
2. Lewis SM, Evans JW, Jalowayski AA. Continuous distributions of specific ventilation recovered from inert gas washout. J Appl Physiol Respir Environ Exerc Physiol. 1978; 44(3):416–23. [PubMed: 632182]
3. Simon BA, Kaczka DW, Bankier AA, Parraga G. What can computed tomography and magnetic resonance imaging tell us about ventilation? J Appl Physiol (1985). 2012; 113(4):647–57. [PubMed: 22653989]
4. Tzeng YS, Lutchen K, Albert M. The difference in ventilation heterogeneity between asthmatic and healthy subjects quantified using hyperpolarized 3He MRI. J Appl Physiol (1985). 2009; 106(3): 813–22. [PubMed: 19023025]
5. Verbanck S, Thompson BR, Schuermans D, et al. Ventilation heterogeneity in the acinar and conductive zones of the normal ageing lung. Thorax. 2012; 67(9):789–95. [PubMed: 22544894]

6. Wagner PD, Saltzman HA, West JB. Measurement of continuous distributions of ventilation-perfusion ratios: theory. J Appl Physiol. 1974; 36(5):588–99. [PubMed: 4826323]
7. Robinson PD, Latzin P, Verbanck S, et al. Consensus statement for inert gas washout measurement using multiple- and single- breath tests. Eur Respir J. 2013; 41(3):507–22. [PubMed: 23397305]
8. Horsley A, Wild JM. Ventilation heterogeneity and the benefits and challenges of multiple breath washout testing in patients with cystic fibrosis. Paediatr Respir Rev. 2015; 16(Suppl 1):15–8. [PubMed: 26420586]
9. Kent L, Reix P, Innes JA, et al. Lung clearance index: Evidence for use in clinical trials in cystic fibrosis. J Cyst Fibros. 2014; 13(2):123–38. [PubMed: 24315208]
10. Horsley A. Lung clearance index in the assessment of airways disease. Resp Med. 2009; 103(6): 793–9.
11. Aurora P, Gustafsson P, Bush A, et al. Multiple breath inert gas washout as a measure of ventilation distribution in children with cystic fibrosis. Thorax. 2004; 59(12):1068–73. [PubMed: 15563707]
12. Edelman RR, Hatabu H, Tadamura E, Li W, Prasad PV. Noninvasive assessment of regional ventilation in the human lung using oxygen-enhanced magnetic resonance imaging. Nat Med. 1996; 2(11):1236–9. [PubMed: 8898751]
13. Ohno Y, Hatabu H, Takenaka D, Van Cauteren M, Fujii M, Sugimura K. Dynamic oxygen-enhanced MRI reflects diffusing capacity of the lung. Magn Reson Med. 2002; 47(6):1139–44. [PubMed: 12111960]
14. Sa RC, Asadi AK, Theilmann RJ, Hopkins SR, Prisk GK, Darquenne C. Validating the distribution of specific ventilation in healthy humans measured using proton MR imaging. J Appl Physiol. 2014; 116(8):1048–56. [PubMed: 24505099]
15. Halaweish AF, Moon RE, Foster WM, et al. Perfluoropropane Gas as a Magnetic Resonance Lung Imaging Contrast Agent in Humans. Chest. 2013; 144(4):1300–10. [PubMed: 23722696]
16. Ouriadov AV, Fox MS, Couch MJ, Li T, Ball IK, Albert MS. In vivo regional ventilation mapping using fluorinated gas MRI with an x-centric FGRE method. Magn Reson Med. 2015; 74(2):550–7. [PubMed: 25105721]
17. Salerno M, Altes TA, Mugler JP 3rd, Nakatsu M, Hatabu H, de Lange EE. Hyperpolarized noble gas MR imaging of the lung: potential clinical applications. Eur J Radiol. 2001; 40(1):33–44. [PubMed: 11673006]
18. de Lange EE, Altes TA, Patrie JT, et al. Evaluation of asthma with hyperpolarized helium-3 MRI: correlation with clinical severity and spirometry. Chest. 2006; 130(4):1055–62. [PubMed: 17035438]
19. Costella S, Kirby M, Maksym GN, McCormack DG, Paterson NA, Parraga G. Regional pulmonary response to a methacholine challenge using hyperpolarized 3He magnetic resonance imaging. Respirology. 2012; 17(8):1237–46. [PubMed: 22889229]
20. Kirby M, Svenningsen S, Owrangi A, et al. Hyperpolarized 3He and 129Xe MR imaging in healthy volunteers and patients with chronic obstructive pulmonary disease. Radiology. 2012; 265(2):600–10. [PubMed: 22952383]
21. Svenningsen S, Kirby M, Starr D, et al. What are ventilation defects in asthma? Thorax. 2014; 69(1):63–71. [PubMed: 23956019]
22. Fain SB, Gonzalez-Fernandez G, Peterson ET, et al. Evaluation of structure-function relationships in asthma using multidetector CT and hyperpolarized He-3 MRI. Acad Radiol. 2008; 15(6):753–62. [PubMed: 18486011]
23. Altes TA, Powers PL, Knight-Scott J, et al. Hyperpolarized 3He MR lung ventilation imaging in asthmatics: preliminary findings. J Magn Reson Imaging. 2001; 13(3):378–84. [PubMed: 11241810]
24. Mugler JP 3rd, Altes TA. Hyperpolarized 129Xe MRI of the human lung. J Magn Reson Imaging. 2013; 37(2):313–31. [PubMed: 23355432]
25. Virgincar RS, Cleveland ZI, Kaushik SS, et al. Quantitative analysis of hyperpolarized 129Xe ventilation imaging in healthy volunteers and subjects with chronic obstructive pulmonary disease. NMR Biomed. 2013; 26(4):424–35. [PubMed: 23065808]

26. Stewart NJ, Norquay G, Griffiths PD, Wild JM. Feasibility of human lung ventilation imaging using highly polarized naturally abundant xenon and optimized three-dimensional steady-state free precession. Magn Reson Med. 2015; 74(2):346–52. [PubMed: 25916276]
27. Kirby M, Svenningsen S, Kanhere N, et al. Pulmonary ventilation visualized using hyperpolarized helium-3 and xenon-129 magnetic resonance imaging: differences in COPD and relationship to emphysema. J Appl Physiol. 2013; 114(6):707–15. [PubMed: 23239874]
28. Svenningsen S, Kirby M, Starr D, et al. Hyperpolarized 3He and 129Xe MRI: differences in asthma before bronchodilation. J Magn Reson Imaging. 2013; 38(6):1521–30. [PubMed: 23589465]
29. Woodhouse N, Wild JM, Paley MN, et al. Combined helium-3/proton magnetic resonance imaging measurement of ventilated lung volumes in smokers compared to never-smokers. J Magn Reson Imaging. 2005; 21(4):365–9. [PubMed: 15779032]
30. Kirby M, Heydarian M, Svenningsen S, et al. Hyperpolarized 3He magnetic resonance functional imaging semiautomated segmentation. Acad Radiol. 2012; 19(2):141–52. [PubMed: 22104288]
31. He M, Kaushik SS, Robertson SH, et al. Extending semiautomatic ventilation defect analysis for hyperpolarized (129)Xe ventilation MRI. Acad Radiol. 2014; 21(12):1530–41. [PubMed: 25262951]
32. Hahn AD, Cadman RV, Sorkness RL, Jarjour NN, Nagle SK, Fain SB. Redistribution of inhaled hyperpolarized He3 gas during breath-hold differs by asthma severity. J Appl Physiol. 1985 2015:jap 00197 2015.
33. Ebner L, He M, Virgincar RS, et al. Hyperpolarized 129Xenon MRI to Quantify Regional Ventilation Differences in Mild to Moderate Asthma: A Prospective Comparison between SemiAutomated Ventilation Defect Percentage Calculation and Pulmonary Function Tests. Invest Radiol. 2016 (Submitted).
34. He M, Robertson SH, Kaushik SS, et al. Dose and pulse sequence considerations for hyperpolarized (129)Xe ventilation MRI. Magn Reson Imaging. 2015; 33(7):877–85. [PubMed: 25936684]
35. Fulambarker A, Copur AS, Javet A, Jere S, Cohen ME. Reference values for pulmonary function in Asian Indians living in the United States. Chest. 2004; 126(4):1225–33. [PubMed: 15486386]
36. Kirby M, Mathew L, Wheatley A, Santyr GE, McCormack DG, Parraga G. Chronic obstructive pulmonary disease: longitudinal hyperpolarized 3He MR imaging. Radiology. 2010; 256(1):280–9. [PubMed: 20574101]
37. Hamerly, G., Elkan, C. Neural Information Processing Systems. MIT Press; 2003. Learning the K in K-Means.
38. MacKay, DJC. Reprinted with corrections. Cambridge, UK ; New York: Cambridge University Press; 2004. Information theory, inference, and learning algorithms.
39. Deninger AJ, Mansson S, Petersson JS, et al. Quantitative measurement of regional lung ventilation using He-3 MRI. Magn Reson Med. 2002; 48(2):223–32. [PubMed: 12210930]
40. Emami K, Kadlecek SJ, Woodburn JM, et al. Improved technique for measurement of regional fractional ventilation by hyperpolarized 3He MRI. Magn Reson Med. 2010; 63(1):137–50. [PubMed: 19877277]
41. Horn FC, Deppe MH, Marshall H, Parra-Robles J, Wild JM. Quantification of regional fractional ventilation in human subjects by measurement of hyperpolarized 3He washout with 2D and 3D MRI. J Appl Physiol (1985). 2014; 116(2):129–39. [PubMed: 24311749]
42. Hamedani H, Clapp JT, Kadlecek SJ, et al. Regional Fractional Ventilation by Using Multibreath Wash-in 3He MR Imaging. Radiology. :150495.
43. Sa RC, Cronin MV, Henderson AC, et al. Vertical distribution of specific ventilation in normal supine humans measured by oxygen-enhanced proton MRI. J Appl Physiol (1985). 2010; 109(6): 1950–9. [PubMed: 20930129]
44. Sheikh K, Paulin GA, Svenningsen S, et al. Pulmonary ventilation defects in older never-smokers. J Appl Physiol (1985). 2014; 117(3):297–306. [PubMed: 24903918]
45. Janssens JP, Pache JC, Nicod LP. Physiological changes in respiratory function associated with ageing. Eur Respir J. 1999; 13(1):197–205. [PubMed: 10836348]

46. Cardus J, Burgos F, Diaz O, et al. Increase in pulmonary ventilation-perfusion inequality with age in healthy individuals. Am J Respir Crit Care Med. 1997; 156(2 Pt 1):648–53. [PubMed: 9279253]
47. Heckscher T, Bass H, Oriol A, Rose B, Anthoniesen NR, Bates DV. Regional lung function in patients with bronchial asthma. J Clin Invest. 1968; 47(5):1063–70. [PubMed: 5645852]
48. Gompelmann D, Eberhardt R, Herth FJ. Collateral ventilation. Respiration; international review of thoracic diseases. 2013; 85(6):515–20. [PubMed: 23485627]
49. Macklem PT. Airway obstruction and collateral ventilation. Physiological reviews. 1971; 51(2): 368–436. [PubMed: 4928122]
50. Kaminsky DA, Bates JH, Irvin CG. Effects of cool, dry air stimulation on peripheral lung mechanics in asthma. Am J Respir Crit Care Med. 2000; 162(1):179–86. [PubMed: 10903239]
51. Moore WC, Meyers DA, Wenzel SE, et al. Identification of Asthma Phenotypes Using Cluster Analysis in the Severe Asthma Research Program. Am J Respir Crit Care Med. 2010; 181(4):315–23. [PubMed: 19892860]
52. Despas PJ, Leroux M, Macklem PT. Site of airway obstruction in asthma as determined by measuring maximal expiratory flow breathing air and a helium-oxygen mixture. J Clin Invest. 1972; 51(12):3235–43. [PubMed: 4640957]
53. Lagerstrand L, Skedinger M, Ihre E, Hallden G, Zetterstrom O. Spirometry and ventilation-perfusion inequality in patients with mild allergic asthma before and during the pollen season. Clin Physiol. 1995; 15(4):355–64. [PubMed: 7554770]
54. Cardus J, Burgos F, Diaz O, et al. Increase in pulmonary ventilation-perfusion inequality with age in healthy individuals. Am J Respir Crit Care Med. 1997; 156(2):648–53. [PubMed: 9279253]
55. Macleod KA, Horsley AR, Bell NJ, Greening AP, Innes JA, Cunningham S. Ventilation heterogeneity in children with well controlled asthma with normal spirometry indicates residual airways disease. Thorax. 2009; 64(1):33–7. [PubMed: 18678703]
56. Kraemer R, Blum A, Schibler A, Ammann RA, Gallati S. Ventilation inhomogeneities in relation to standard lung function in patients with cystic fibrosis. Am J Resp Crit Care. 2005; 171(4):371–8.

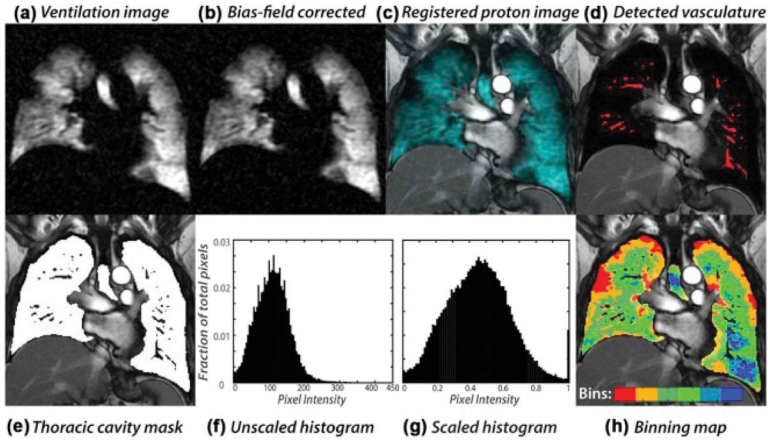

Figure 1.

(a) ^{129}Xe MRI as acquired. (b) after correction for B1 inhomogeneity. (c) ^{1}H thoracic cavity image registered to ^{129}Xe MRI. (d) Detection of vascular structures within the ^{1}H image. (e) Segmentation and 1 pixel erosion to create a thoracic cavity mask with vascular structures removed, (f) histogram of ^{129}Xe intensities within the mask, (f) ^{129}Xe histogram after rescaling by the top percentile of all intensities. (h) Binning map generated after applying thresholds.

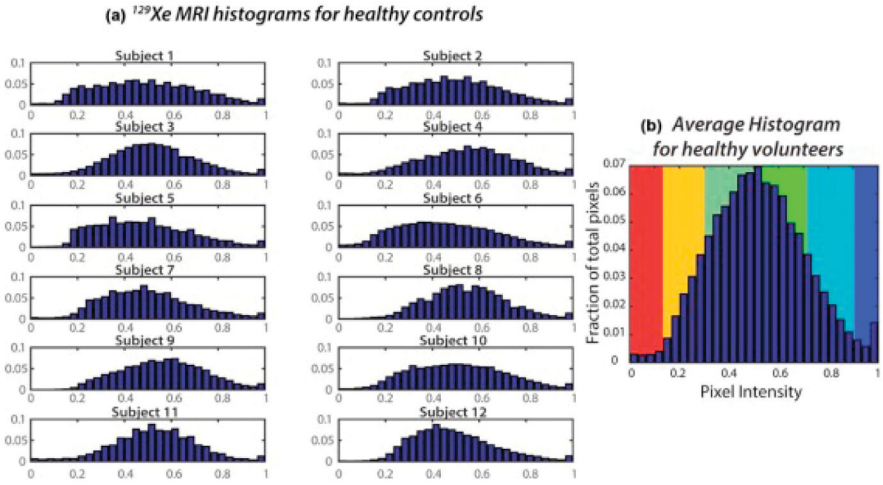

Figure 2.

(A) Rescaled ventilation distribution for the 10 young normal individuals. (B) Average distribution for the 10 subjects has a mean of 0.52 and SD of 0.18. This was used to define the thresholds and widths of 6 bins used to quantify and map the ventilation distribution.

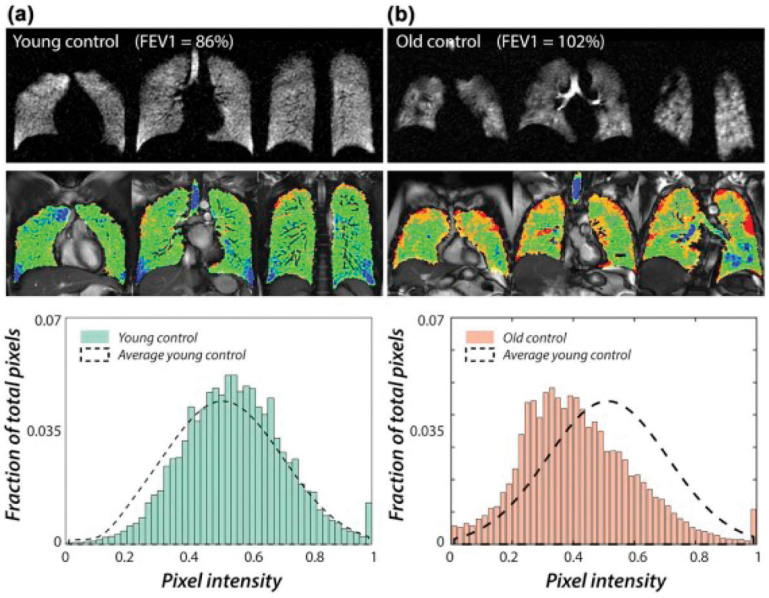

Figure 3.

Examples of ^{129}Xe-derived ventilation distributions in a younger and older normal subject. (A) In a 27-year-old healthy subject with FEV1of 86%, the ^{129}Xe ventilation image shows very few ventilation defects. The associated histogram is similar to that of normal young controls, with mean of 0.54 and SD of 0.18. (B) In a 58-year-old healthy subject with FEV1 of 102%, the ventilation image shows areas of ventilation defects (red) and low ventilation (orange). The associated ventilation histogram shifted towards lower values compared to that of normal young controls, with a mean of 0.40 and SD of 0.20.

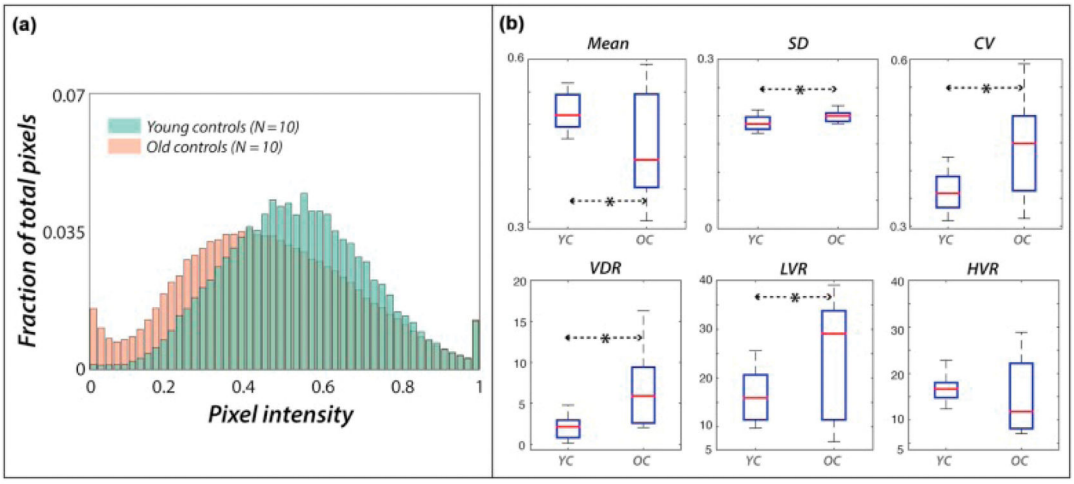

Figure 4.

Comparison of ventilation distribution parameters between the younger and the older control groups. (A) Ventilation distribution histogram from the older control (OC) group (red) is overlaid with that from the young control (YC) group (blue). The ventilation distribution in the older healthy subjects shifted towards lower values compared to the younger group. (B) Comparison of ventilation distribution parameters between the young and the old groups shows significant differences for all parameters except HVR. (*- indicates $p \leq 0.05$.)

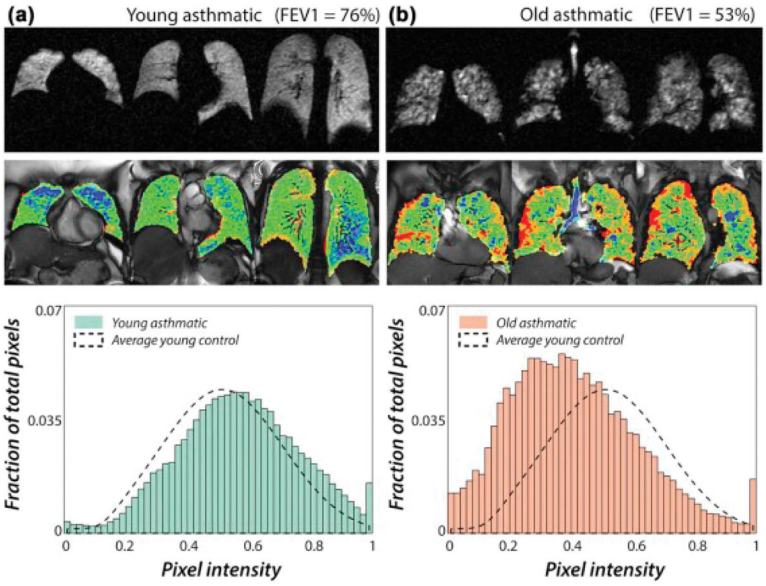

Figure 5.

Representative ventilation distributions in a younger and older asthma subject. (A) The younger asthma subject with FEV1of 76% exhibits a ventilation image with very few ventilation defects. The associated histogram is similar to that of normal young controls. (B) The older asthma subject with FEV1 of 53% has a ventilation image with significant areas of ventilation defects (red) and low ventilation (orange). The associated ventilation histogram was significantly right-skewed compared to that of normal young controls.

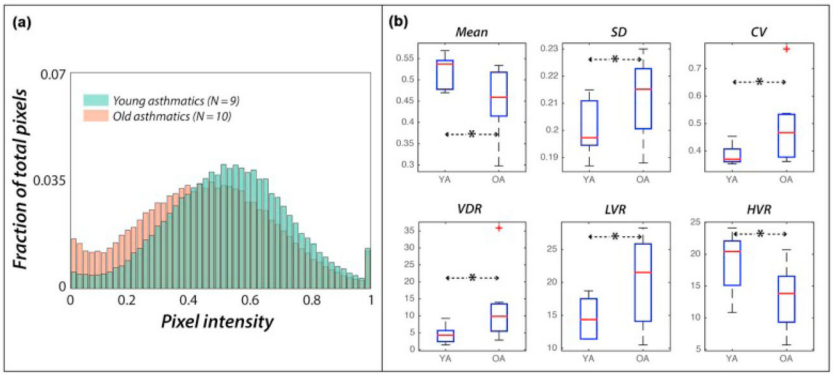

Figure 6.

Comparison of ventilation distributions between the younger and the older asthma groups. (A) Ventilation distribution histogram from the older asthma (OA) group (red) is overlaid with that from the younger asthma (YA) group (blue). In the older asthma group the distribution is shifted towards lower values compared to the younger asthmatics. (B) Comparison of ventilation distribution parameters between the younger and the older asthma groups shows significant differences in all parameters * $p \leq 0.05$.

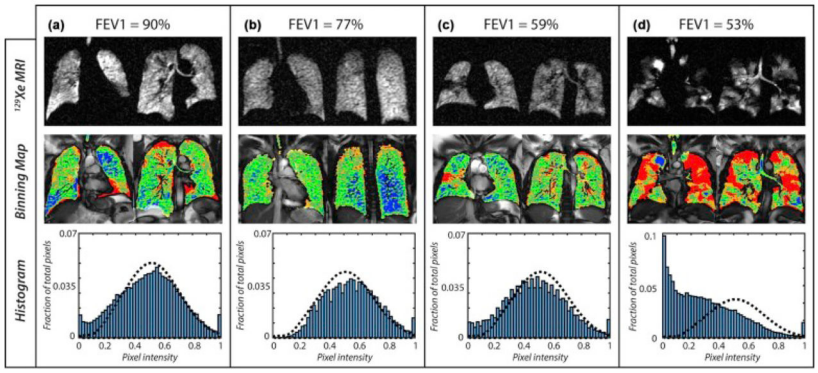

Figure 7.

Comparisons between FEV1 and ^{129}Xe MRI-derived ventilation distribution in patients with asthma. (A) A patient with normal FEV1, but abnormal ^{129}Xe MRI. (B) A patient with abnormal FEV1, but normal ^{129}Xe MRI. (C) and (D) Two patients with moderate asthma with similarly low FEV1, but markedly different ventilation patterns.

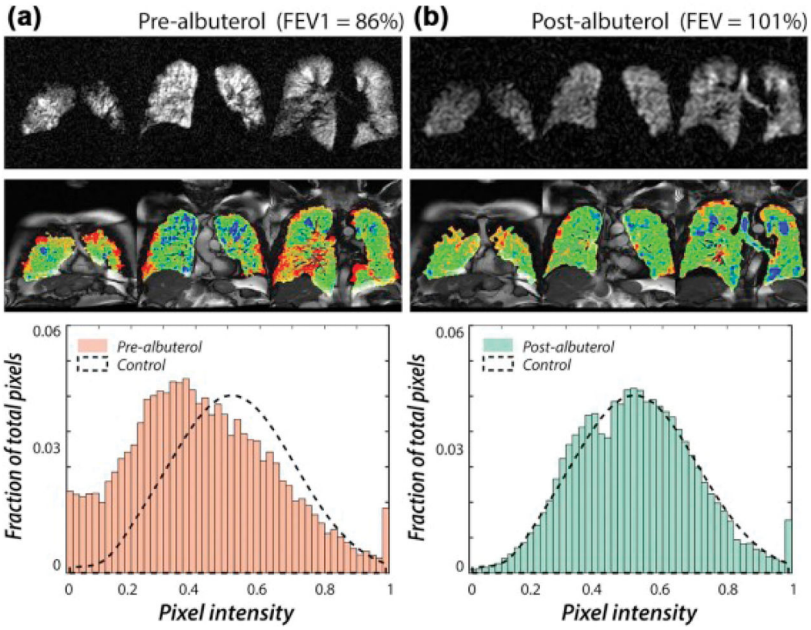

Figure 8.

Ventilation distribution in a patient with mild intermittent asthma who had positive bronchodilator response to albuterol based on FEV1 criteria. (A) The binning map (top) and histogram (bottom) before albuterol. (B) The binning map (top) and histogram (bottom) after albuterol showed decreased VDR and LVR, and a distribution matching that of young normal controls after bronchodilator.

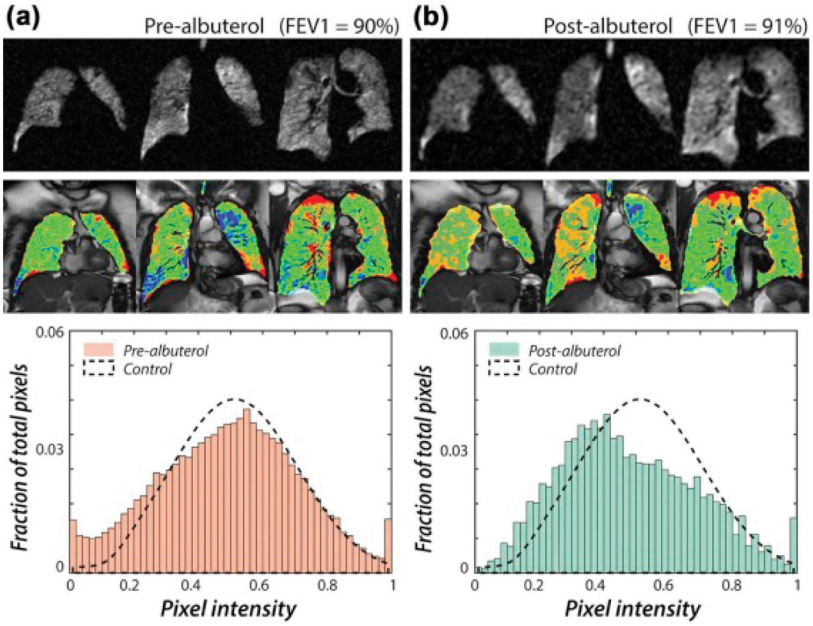

Figure 9.

Ventilation distribution in a patient with mild intermittent asthma who did not respond to albuterol based on FEV1 criteria. (A) The binning map (top) and histogram (bottom) before albuterol. (B) The binning map (top) and histogram (bottom) after albuterol. The ventilation distribution histogram after albuterol showed decreased VDR but increased LVR at the expense of normally ventilated regions. This may be the result of more normal airways dilating and redistributing ventilation.